Braz J Phys (2014) 44:494–503
DOI 10.1007/s13538-014-0220-z

SOCIEDADE BRASILEIRA DE FÍSICA

PARTICLES AND FIELDS

Highlights of the ARGO-YBJ Experiment at 4,300 m a.s.l.

Zhen Cao for The ARGO-YBJ Collaboration

Received: 28 April 2014 / Published online: 6 June 2014

Abstract The ARGO-YBJ experiment in Tibet, China has been operated to survey the northern sky for gamma ray sources, transient or steady, for nearly 6 years. Many astrophysics observational results will be highlighted in this paper, such as the sky survey results, extended source observation, diffuse gamma rays from the galactic plane, and emission mechanism of AGNs and their flares. As the unique detector for EAS with a continuously sensitive area of 5,600 m^2, the ARGO-YBJ array catches almost all particles in the central part of showers. The high-quality data set for showers above few TeV has been used for cosmic ray measurements such as the energy spectrum and composition. All those results are summarized here. As one of the next generation ground-based high-altitude air shower detector, LHAASO is briefly introduced as the successor of ARGO-YBJ in the end of the paper.

Keywords AGN · Gamma ray source · Energy spectrum · Composition · RPC

1 ARGO-YBJ as a Cosmic Ray and Gamma Ray Observatory

ARGO-YBJ is an experiment measuring extensive air shower (EAS) of cosmic rays and very high energy (VHE) gamma rays in a field of view about 50° respect to the zenith. Located at Yangbajing Cosmic Ray Observatory at 4,300 m a.s.l. about 90 km from the capital city Lhasa of Tibet, China, the detector consists of a single layer of resistive plate chambers (RPCs) of 5,600 m^2 in total. Each of the RPC is about 3 m^2, equipped with pick-up strips (6.75 cm × 61.80 cm each) that return bits as the charged particle(s) passing through. The particle(s) are also timed by a TDC attached to every 8 strips with a resolution of about 1.8 ns which is sufficient to measure the EAS direction in a fraction of degree as more than 100 hits are recorded. The detector is continuously operated clock round and monitors the northern sky with the rotation of the earth in day and night [1, 2]. In order to count the number of particles on a RPC in big showers, each RPC is also equipped with two 12-bit ADC read out channels for induced charges in both halves of the chamber [3, 4]. The angular resolution, pointing accuracy, and stability of the ARGO-YBJ detector array have been thoroughly tested by measuring the shadow of the Moon in cosmic rays with a significance of more than 80σ. The point-spread function (PSF) is quantified by the parameter Ψ_{70}, the opening angle of the cone containing 71.5 % of the events from a point source, to be 0.47° at $N_{hit} > 1,000$ and 2.8° at $N_{hit} > 20$ [5]. The westward shift of the shadow due to the geomagnetic field has been used to calibrate the shower energy measurement by taking the advantage of very precise measurements of the geomagnetic field. The absolute energy scale is determined to be better than 13 % [6], in which 7 % is due to the lack of the precise knowledge about the composition of the cosmic rays.

2 Gamma Ray Observations

The ARGO-YBJ data used in this analysis were collected from November 2007 to January 2013. The total effective observation time is 1,670.45 days. As the standard candle in the northern sky, the Crab Nebula is observed with a

Z. Cao (✉) · The ARGO-YBJ Collaboration
Key Laboratory of Particle Astrophysics, Institute of High Energy Physics, Chinese Academy of Sciences, P.O. Box 918, 100049 Beijing, People's Republic of China
e-mail: caozh@ihep.ac.cn

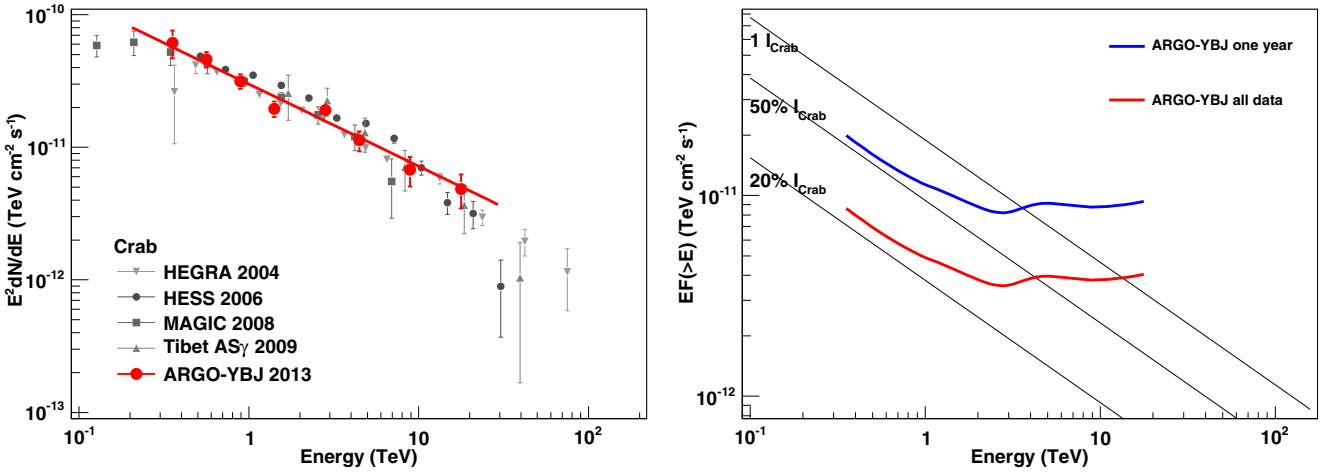

Fig. 1 *Left*: Differential energy spectrum of the Crab Nebula measured by ARGO-YBJ [17] and comparison with the measurements of HEGRA, HESS, MAGIC, and Tibet AS [33–35]. The *solid line* is the best fit to ARGO-YBJ data using a power-law function. *Right*: Differential and integrated sensitivity of the ARGO-YBJ detector with a total exposure of 1,600 h in the last 5 years

significance of 21 standard deviation(SD), corresponding to an integrated sensitivity of 24 $\%I_{Crab}$ and differential sensitivity of 55 $\%I_{Crab}/year$. Many experiments have measured the spectral energy distribution (SED) of this nearly perfect point source. The results are in very good agreement with our measurement as shown in the left panel of Fig. 1 [7]. The pointing uncertainty is found to be better than 0.1°. Both differential and integrated sensitivities by the end of 2012 are plotted in the right panel of Fig. 1.

2.1 Galactic Steady Emitters: Extended and Diffused

As a device with a wide field of view (FOV), ARGO-YBJ handles the background estimation for extended sources more reliably than the Cherenkov telescopes that have narrower FOV. Sources, HESS J1908+063, MGRO J2031+41, and HESS J1841-055 are observed with significance above 5.3σ. With the spatial extension of 0.5, 0.4, and 0.2°, respectively, in terms of the standard deviation of the two-dimensional Gaussian, the fluxes of the sources are all measured higher than what is reported by the Cherenkov telescope experiments. As examples, the comparison of HESS J1908+063 and MGRO J2031+41 SEDs with the corresponding measurements by telescopes are shown in Fig. 2 [8]. All the observations demonstrate the fact that a wide FOV detector, such as ARGO-YBJ, is more sensitive for extended sources than pointing devices because of the better signal-to-noise ratio. This opens an important window

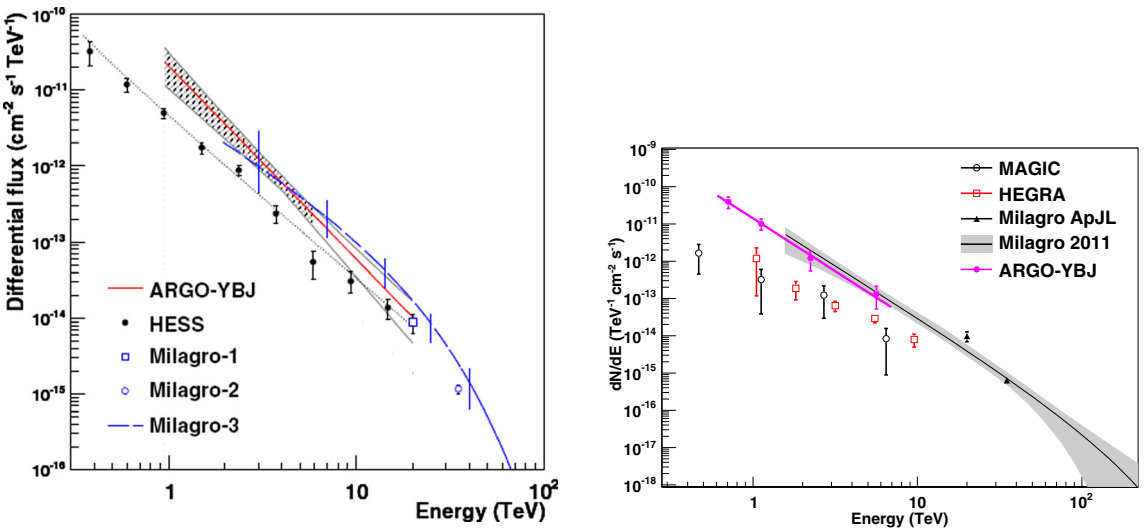

Fig. 2 SED's of extended galactic sources, HESS J1908+063 (*left*), MGRO J2031+41 (i.e., TeV J2032+4130) (*right*), measured by ARGO-YBJ compared with the corresponding measurements by Cherenkov telescopes

for discovering more sources with spatial extension. Those sources could be very interesting in searching for the origin of CR particles. In many occasions, the accelerator of charged particles could be spatially separated from the target region where the gamma rays are produced. Discovering more such kind of sources and very detailed observations on them are particularly useful in searches for the cosmic accelerators.

MGRO J2031+41, overlapping with TeV J2032+4130, is almost at the center of FERMI "Cocoon" which is well measured by FERMI [9] as a very bright rather large area in the very active Cygnus region associated with the super-bubble. MILAGRO measured this source as a quite extended source. Without sufficient energy resolution, MILAGRO measured the flux over a wide energy range centered at slightly higher energy than 10 TeV. This is quite a unique measurement at high energy. Between this measurement and FERMI one at energies from few GeV to 100 GeV, ARGO-YBJ makes an essential contribution in filling the gap of the spectrum of gamma rays from the blob. Around the observed source as ARGO J2031+4157 listed in Table 1 by ARGO-YBJ, the spectrum in a region of $3^\circ \times 3^\circ$ is shown in Fig. 3. as a preliminary result by using ARGO-YBJ data. The spectrum makes a nearly smooth connection between the two experiments, FERMI and MILAGRO. Further studies aiming at improving the understanding on the emission mechanism in the "Cocoon" is undergoing. The fitting of the spectrum obtained from the multiwavelength analysis is not trivial.

Near the FERMI "Cocoon," MILAGRO found its brightest source MGRO J2019+37, a spatially quite extended source. Although it has a total flux of about 80 $\%I_{Crab}$, this source was not detected by any Cherenkov telescope experiment. Not only for the telescopes, ARGO-YBJ also missed this source at all [10]. This source is therefore very special in terms of the SED, which is extremely hard, see Fig. 4. The gamma ray emission only occur in a narrow band peaked around 20 TeV, according to the limits set by ARGO-YBJ and the observation by MILAGRO. Such a sharp peak could be difficult to model if an electron-dominant origin is assumed. FERMI data seems to provide further evidence because no strong emission is found in this direction in FERMI data. The limits have been drawn on the same figure. Further down to the lower energy bands, we investigate the X-ray observational data, one found nothing significant in the existing data, such as INTEGRAL which seems not sufficiently sensitive according to the limits in the same figure. More INTEGRAL data are under analysis and data from more sensitive experiments such as NEWTON are also under analysis. The fact, namely that there is no significant emission below 10 TeV, may indicate a very interesting candidate for cosmic ray source.

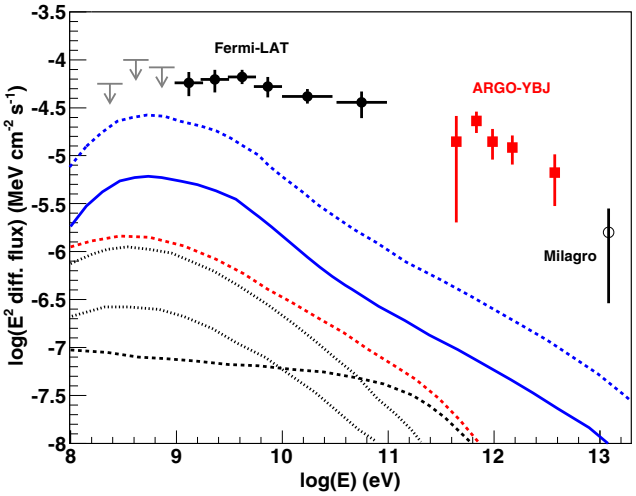

Fig. 3 SED's of FERMI cocoon, overlapping with MGRO J2031+41, also recognized as ARGO J2031+4157, are measured by FERMI at few GeV, in $3^\circ \times 3^\circ$ by ARGO-YBJ below 10 TeV and MILAGRO above 10 TeV. The connection from the experiments at different energies seems quite smooth. Attempts of explanation for the gamma emission have been made, e.g., the curves in the Fig. [9]. No model fits the SED well, yet

Table 1 Location of the excess regions

ARGO-YBJ Name	Ra (°)	Dec (°)	l (°)	b (°)	S (s.d.)	Associated TeV source
ARGO J0409−0627	62.35	−6.45	198.51	−38.73	4.8	
ARGO J0535+2203	83.75	22.05	184.59	−5.67	20.8	Crab Nebula
ARGO J1105+3821	166.25	38.35	179.43	65.09	14.1	Mrk 421
ARGO J1654+3945	253.55	39.75	63.59	38.80	9.4	Mrk 501
ARGO J1839−0627	279.95	−6.45	25.87	−0.36	6.0	HESS J1841−055
ARGO J1907+0627	286.95	6.45	40.53	−0.68	5.3	HESS J1908+063
ARGO J1910+0720	287.65	7.35	41.65	−0.88	4.3	
ARGO J1912+1026	288.05	10.45	44.59	0.20	4.2	HESS J1912+101
ARGO J2021+4038	305.25	40.65	78.34	2.28	4.3	VER J2019+407
ARGO J2031+4157	307.95	41.95	80.58	1.38	6.1	MGRO J2031+41
						TeV J2032+4130
ARGO J1841−0332	280.25	−3.55	28.58	0.70	4.2	HESS J1843−033

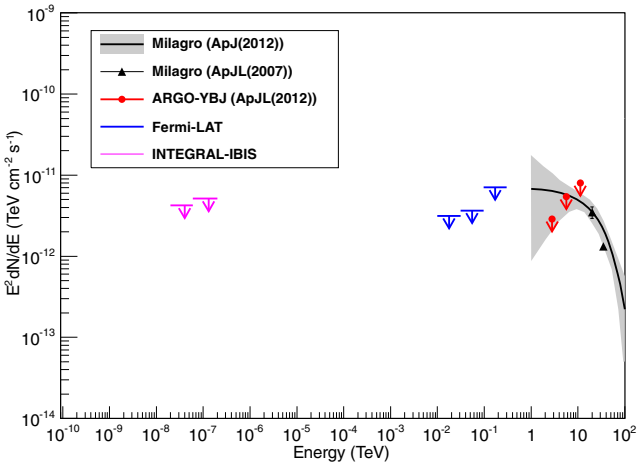

Fig. 4 SED's of MGRO J2019+37 and all upper limits at all energies below 20 TeV

The diffuse gamma rays from the galactic plane have a clear origin, namely the decay products of π^0 produced in collisions with gases and dusts, electromagnetic origin via bremsstrahlung, and inverse Compton processes of cosmic rays during the propagation in the galactic disk. In the northern sky map made of all ARGO-YBJ events, an excess along the galactic plane is observed as expected. Integrating over a belt $\pm 5°$ along the galactic plane, the excess has a distribution over galactic longitudes l, being the observed excess rather significant in the region $l < 110°$, but not in the region so-called outer disk ($l > 130°$). The excess seems to concentrate towards 75° in the direction of the Cygnus region. Integrating over the most significant region, from the lower boundary of the ARGO-YBJ FOV 25 to 85°, the excess has a clear profile along the galactic latitude, z, and peaks up at $z = 0$. A particular attention has been given to the Cygnus region in the spectroscopic analysis, where FERMI has done a detailed analysis as well [11]. Since the excess drops rather fast with latitude z, as mentioned, the average flux is strongly depending on the width of the belt along the plane, in which the observations are carried out by different experiments, e.g., FERMI in $\pm 15°$, MILAGRO in $\pm 2°$ [12], and ARGO-YBJ in $\pm 5°$. In order to compare the results of different experiments, a prediction about the diffuse gamma ray flux based on some basic assumptions on the cosmic ray propagation through our galaxy and distributions of all gases on the disk is adopted according to FERMI, who fitted the prediction with its data in the double belts 10° away from the disk, i.e., $10° < |z| < 15°$. In the Cygnus region, namely $65° < l < 85°$, the diffuse gamma ray flux measured by ARGO-YBJ around 1 TeV agrees with the prediction pretty well, while the same prediction seems to fit FERMI data in $\pm 15°$ well above 3 GeV, but seems to be slightly underestimated below. One may conclude that the flux is quite consistent with the conventional assumption of CR propagation model, while MILAGRO observes a flux at 15 TeV significantly at variance with the prediction. In the other longitude range, on the other hand, no strong excess over the prediction has been observed by ARGO-YBJ. To remind readers about the historic measurements, experimental results by Whipple [13], HEGRA [14], AS$_\gamma$, and MILAGRO are plotted in the same figure. Their relatively high limits indicate the insufficient sensitivities of the detectors. MILAGRO is consistent with the

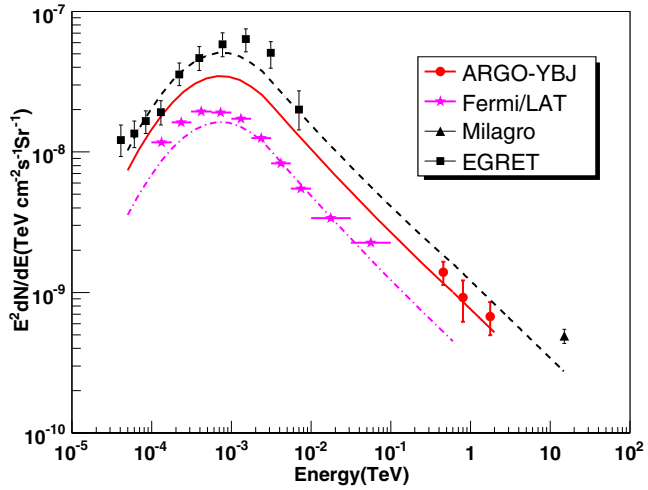

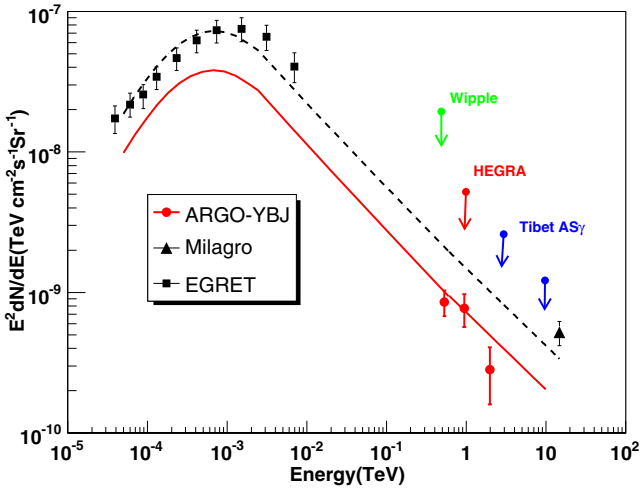

Fig. 5 SED's of diffuse gamma rays from the galactic plane. *Left*: In the longitude range centered at Cygnus region, i.e., $65° < l < 85°$, FERMI and MILAGRO data at low- and high-energy ends are plotted for comparison. *Lines* are predicted average fluxes in belts of $\pm 15°$ for FERMI in *dash-dotted*, $\pm 5°$ for ARGO-YBJ in *solid*, and $\pm 2°$ for MILAGRO in *dashed*. *Right*: diffuse gamma ray fluxes from the galactic plane in the region of $25° < l < 65°$ and $85° < l < 100°$. Similar in the left panel, the predictions corresponding to belts of $\pm 5°$ for ARGO-YBJ and $\pm 2°$ for other experiments are plotted. Except MILAGRO which observed the flux above 10 TeV marked by the *black triangle*; all other experiments, such as Whipple, HEGRA, and AS$_\gamma$, only set upper limits

prediction within 1.5σ, and agrees with a simple power-law extension from the well-known EGRET results around 1 GeV, as shown in Fig. 5.

2.2 Outside Our Galaxy: Flares of AGNs and Their Spectrum Evolution

Following the long observation of very active periods of Mrk421 for years since 2006, ARGO-YBJ caught a couple significant flares of Mrk501 which has been so quiet since 1997. By the long cumulative detection of both AGNs with significance of 13.9σ and 9.1σ, respectively, the gamma ray emission of the blazars seems to be quite favorable to the SSC mechanism [15]. The fitting using a simple one-zone model to the multiwavelength observational data covering X-ray, gamma ray, and very high energy (VHE) bands demonstrates a strong support to the mechanism. Two bumps corresponding to synchrotron radiation below 1 MeV and inverse Compton (IC) scattering above 1 GeV are separated rather clearly, as shown in Fig. 6 [16]. In contrast, very significant hardening of the spectra in both synchrotron and IC domains are observed during flares. The synchrotron and IC spectra become so hard particularly in VHE band that the simple SSC assumption no longer fits the data well enough. The differences between SEDs are clearly seen also in Fig. 6. This implies that the radiation mechanism becomes more complicated during the episodes of TeV flaring. It is very interesting to witness the evolution of the SEDs along with the developments of flares that have long durations. The hardening of the SED occurs at the beginning of big flares rather suddenly. In the following decay phase, the SEDs gradually return to the "normal" shape as same as observed in the low states before flaring. It is rather difficult for AGN models to understand such complex features. While more investigations are still undergoing, there is no doubt that more data on flare monitoring and on observation of the quiet phases are very essential to improve our knowledge about the flare mechanism. It is also particularly demonstrated that the continuous multiwavelength monitoring and corresponding analysis is very necessary.

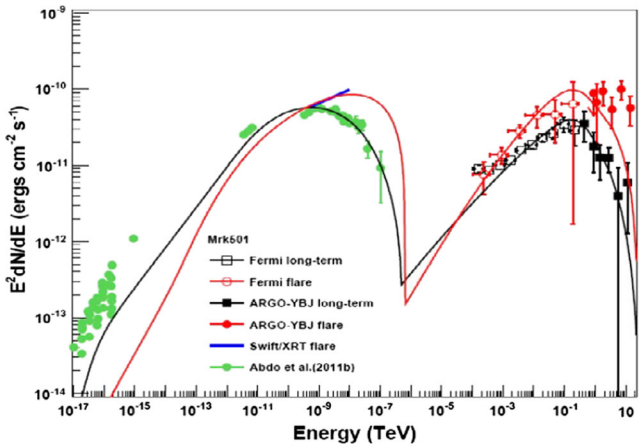

Fig. 6 SED's of Mrk501 during the huge flare in 2010 in *red* at TeV and *blue* at keV versus the SED of steady states measured in THE last few years without significant flares in *green* at keV and in *black* at TeV, respectively. The curves represent the fitting with a simple assumption of SSC mechanism in a single zone

2.3 Sky Survey Results

With the total exposure of 1,670.45 days as mentioned above, ARGO-YBJ surveyed the whole northern sky for steady gamma ray point-like sources to the depth of 24 $\%I_{Crab}$ [17]. Six well-known sources in the VHE gamma ray source catalog have been observed with significance above 5σ, including Crab Nebula and two blazars. Five candidates are observed with significance greater than 4σ. Three of them coincided with known VHE gamma ray sources discovered by VERITAS and HESS, respectively. The remaining two could be potential new sources. The significance of the ARGO-YBJ survey is that the analysis is completely statistically based without any suppression on cosmic ray background by event-by-event gamma-proton separation. All observed sources and candidates are listed in Table 1 below.

3 Cosmic Ray Measurements

At the very high site, the fully covered ARGO-YBJ detector with 93 % active area in the array of 5,600 m^2 measures nearly every charged particle in cosmic ray air showers since the efficiency of the detector is about 97 % [1, 2]. All these features allow ARGO-YBJ to detect showers at energies as low as a few hundred GeV, the same energy region in which balloon-borne detectors such as CREAM [18] are working for direct measurements. This makes the ARGO-YBJ experiment unique among ground-based EAS arrays in terms of being able to be calibrated by directly comparing with the direct measurements. The absolute energy scale in ground-based measurements can be determined. However, it is well known that there still exists a uncertainty in energy determination associated with the unknown composition of recorded EAS events. A typical ground-based experiment, ARGO-YBJ is highly biased towards showers that develop slowly or penetrate deeply in the atmosphere at the lower energy end of the spectrum. Therefore, protons and helium nuclei are more favored than heavier nuclei. Below 100 TeV, for instance, very rarely there exist showers induced by heavy components in the selected samples, as shown in the simulated event distributions in Fig. 7. There are two complementary ways to handle the energy spectrum measurements as described below.

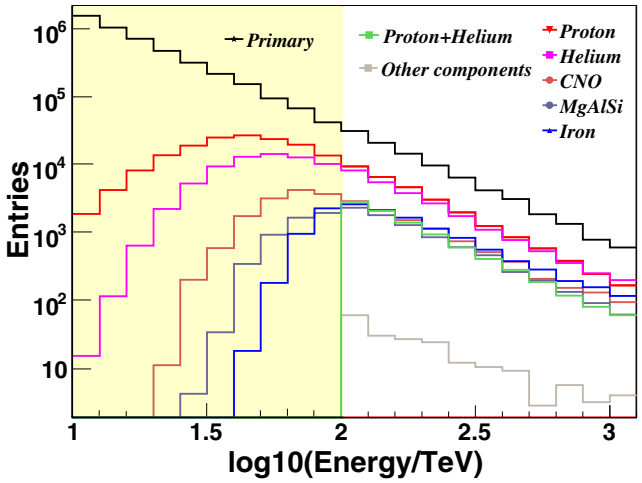

Fig. 7 Simulated energy distributions of ARGO-YBJ events with $N_{hit} > 500$ and cores in the fully covered RPC carpet for assumed composition, i.e., widely used distribution given in [19] among the FIVE components, p, He, C-O-N group, Al-Mg-Si group, and iron, in *red*, *pink*, *brown*, *dark-gray*, and *blue*, respectively. The *black* one is the sum of all the components. Below 100 TeV, trigger bias of the ground-based detector suppresses the heavy components strongly. Above 100 TeV, all species are selected with nearly full efficiency. Using hybrid technique, heavy components can be suppressed sufficiently. The remaining event distribution of the heavy components is in *light-gray* as a contamination less than 2 %. The tradeoff is that the proton and He showers are also cut by 60 %, as shown in *green*

3.1 Energy Scale at 10 TeV

As mentioned at very beginning of this paper, the energy scale can be determined by measuring the westwards drift of the moon shadow position due to the deflection of cosmic rays in the geomagnetic field. However, for showers above 10 TeV, the drift is so small that it cannot be accurately measured. To obtain the energy scale here, matching with the space borne or balloon carried calorimeter experimental results is the essential method. ARGO-YBJ is the unique detector that can carry out the two calibration methods simultaneously. As mentioned above, we have to minimize the uncertainty associated with the unknown composition. In one way, one can take the full advantage of the trigger bias, particularly for showers below 100 TeV, to measure the spectrum of cosmic hydrogen and helium nuclei. In Fig. 7, it is clearly seen that the triggered events are most induced by protons and helium nuclei. The contamination of nuclei heavier than boron is less than 2 % for assumed composition, i.e., widely used distribution given in [19] among the five components, p, He, C-O-N group, Al-Mg-Si group, and iron. In reality, showers with the ARGO-YBJ strip multiplicity greater than 500 are selected. For such a special data set, a Bayesian unfolding method has been developed to "resolve" the energy spectrum using the measured spectrum of strip multiplicity as an input [20]. The spectrum of protons and helium nuclei measured here has been compared with the new result [18] of the CREAM experiment in Fig. 8. Within the statistic errors, which are reasonably small for both experiments below 100 TeV, the two experiments agreed with each other. This is not only simply a measurement of the cosmic ray spectrum but also a very important calibration of the energy scale in the measurement by ground-based ARGO-YBJ array that is calibrated using the moon shadow shifting below 10 TeV. The two calibration agree with each other within 4.5 % at the most.

3.2 Composition Selection: Proton and Helium and Their Spectrum

On the other hand, one could try raising the criteria for event selection to avoid any trigger bias to all species. As shown in Fig. 7, all species can be measured with "full efficiency" in a well-defined aperture, the size of ARGO-YBJ RPC carpet, above 100 TeV. Adding two Cherenkov telescopes [21] to measure the shower image in the sky which is sensitive to the species of the primary particles, the capability of separation between species groups is enhanced. The elongation of the shower image defined as the ratio of the longitudinal and

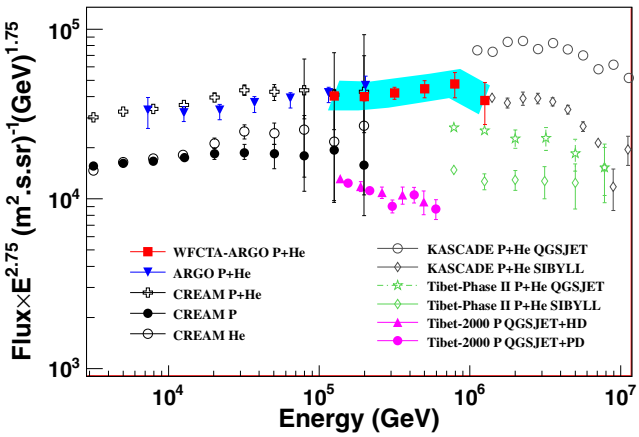

Fig. 8 Spectra of cosmic ray protons and helium nuclei between 3 TeV and 10 PeV. *Blue triangles*, in the range from 10 to 100 TeV, are measured by ARGO-YBJ experiment [20]. The *error bars* are dominated by the systematic uncertainty. The *closed* and *open circles* below 200 TeV are spectra of protons and helium nuclei by CREAM experiment [18]. The *open crosses* are their sum which is compatible with ARGO-YBJ's. The difference between them can be compensated by a difference of 4.5 % in energy scales. The *red squares* below 2 PeV are measured by the hybrid experiment. Statistical errors are represented by *bars* attached to the *squares* and the systematic uncertainties are represented by the *blue belt*. In the similar energy range, the *pink triangles and circles* are measured by AS_γ [25] for "pure protons" with different composition assumptions in the data analysis, respectively. Beyond 1 PeV, measurements by KASCADE [23] in *black* and AS_γ [24] in *green* are plotted for comparison. Different symbols indicate how large the systematic error could be due to the uncertainties in interaction models only

transverse axes is found as a good parameter. The lateral distribution within 2 m from the shower core measured by the RPC carpet is found to be the other good parameter. Combining the two, one demonstrates that an average selection efficiency for protons and α-particles of about 35 % with a contamination of heavier nuclei by 5 % can be achieved. Importantly, the selection does not introduce any bias so that the aperture for protons and αs remains to be a constant with shower energy. For selected protons and αs, their energies are reconstructed using the total numbers of photons in the Cherenkov images. A nearly constant energy resolution of about 25 % over the energy range from 0.1 to 1 PeV is achieved. The energy spectrum is shown in Fig. 8 as the red squares. The results and relevant systematic uncertainties, as shown in the blue belt, are discussed in details elsewhere [22].

It is remarkable that the two measurements using totally different techniques smoothly connect from one to the other, i.e., in the small overlap region around 100 TeV, the difference between the two measurements is less than 2 %, within the systematic errors. The total systematic error of energy scale is less than 10 % in the measurement using total number of registered strips in the RPC carpet. It is mainly due to uncertainties associated with interaction models, composition, selecting criteria, and the detector response, etc. The systematic error using the total number of photons in Cherenkov image is mainly due to the weather condition of 7.6 % and photometric calibration of 5.6 %. Those two measurements cover a very important energy region from 10 TeV to 1 PeV. The spectral index by the hybrid experiment is 2.71 ± 0.06, similar to what is measured by CREAM and ARGO-YBJ (about 2.63) at slightly lower energies. No significant spectral feature, like the knee, is observed below 1 PeV. This result fills the gap between the space/balloon-borne experiments and huge ground array experiments, such as KASCADE [23] and Tibet AS_γ [24] at energies above 1 PeV. They are plotted in the same figure for comparison. Tibet AS_γ also published a spectrum for pure protons [25] at energies between 100 and 700 TeV significantly lower than other measurements and extrapolations. It has a clear steeper index than 2.7. This implies a bending of the spectrum at somewhere lower than 100 TeV.

The hybrid experiment by combining Cherenkov telescopes and RPC array indeed enhanced the capability of the separation between species. The tradeoff is the 10 % duty cycle. Using the ARGO-YBJ full duty cycle data is a way to extend the spectrum above 1 PeV. Even if the selection efficiency for protons and helium is not as good as the hybrid experiment, a similar purity may be achieved because the sample volume is enlarged by a factor of 10. Preliminary progresses have been reported in this conference [26]. Shower ages, determined only by particles in 10 m from the cores, is found to be different by 25 % in average between proton and iron in simulation.

3.3 Anisotropy: Patterns at Different Scales

The anisotropy of cosmic rays over a wide energy region from 0.1 TeV to 1 PeV remains to be a big mystery even if new generation detections offered better 2D view and wider energy coverage [27–29]. ARGO-YBJ plays an important role in the observation of the anisotropy in the following aspects. Annual variation or monthly variation of the spatial pattern of the anisotropy could be a very interesting topic for highly sensitive detectors such as ARGO-YBJ. However, the cosmic ray flux is modulated by the solar activity in the cycle of 11 years. Without a long-term monitoring covering the whole solar cycle, the analysis for the temporal features is difficult. The anisotropy analysis of the ARGO-YBJ data is therefore carried out mainly in the most quiet period of the 23th solar cycle, namely 2008 and 2009, for large-scale anisotropy in particular. The Compton-Getting effect [30], as a well-known harmonic modulation of the flux over the solar time cycle (UT), is caused by the Doppler-like effect of the Earth motion around the Sun in the isotropic "wind" of the galactic cosmic rays. Since it is a pure kinematic effect, it serves as a very precise calibration tool for the ARGO-YBJ detector in terms of the measurement of the anisotropy at a level of few times 10^{-4}. To avoid unclear systematic effects particularly on low-energy events, the high-energy events with multiplicity $N_{hit} > 500$ in the ARGO-YBJ data set are used in the analysis for the Compton-Getting effect observation. Preliminary results for events are shown in Fig. 9, including the 2-D sky maps of the flux variation and corresponding significance as well as the 1D periodical modulation of the integrated flux over the whole observed declination range.

As summarized elsewhere [7], ARGO-YBJ data covers a wide energy range and finds a clear energy dependence of the amplitude of the anisotropy. The most pronouncing anisotropy is found at about 6 TeV. There is no convincing explanation about the energy dependence, yet.

The other important progress in the last 2 years is an analysis of the anisotropy at different spatial scales. Some structures in the sky map at various scales are revealed in the dedicated analysis. The measurements are highlighted because of the coincidences with other experiments at different geographic locations in the world, particularly with IceCube [29], which watches over the southern hemisphere at the large scales, and with MILAGRO [28] in the similar regions of the sky at smaller scales. A full coverage simultaneously using two identical detectors at both hemispheres is nearly the only way to construct a unbiased global view of the anisotropy at large scales. Putting the dipole and quadruple harmonic components of the anisotropy measured by

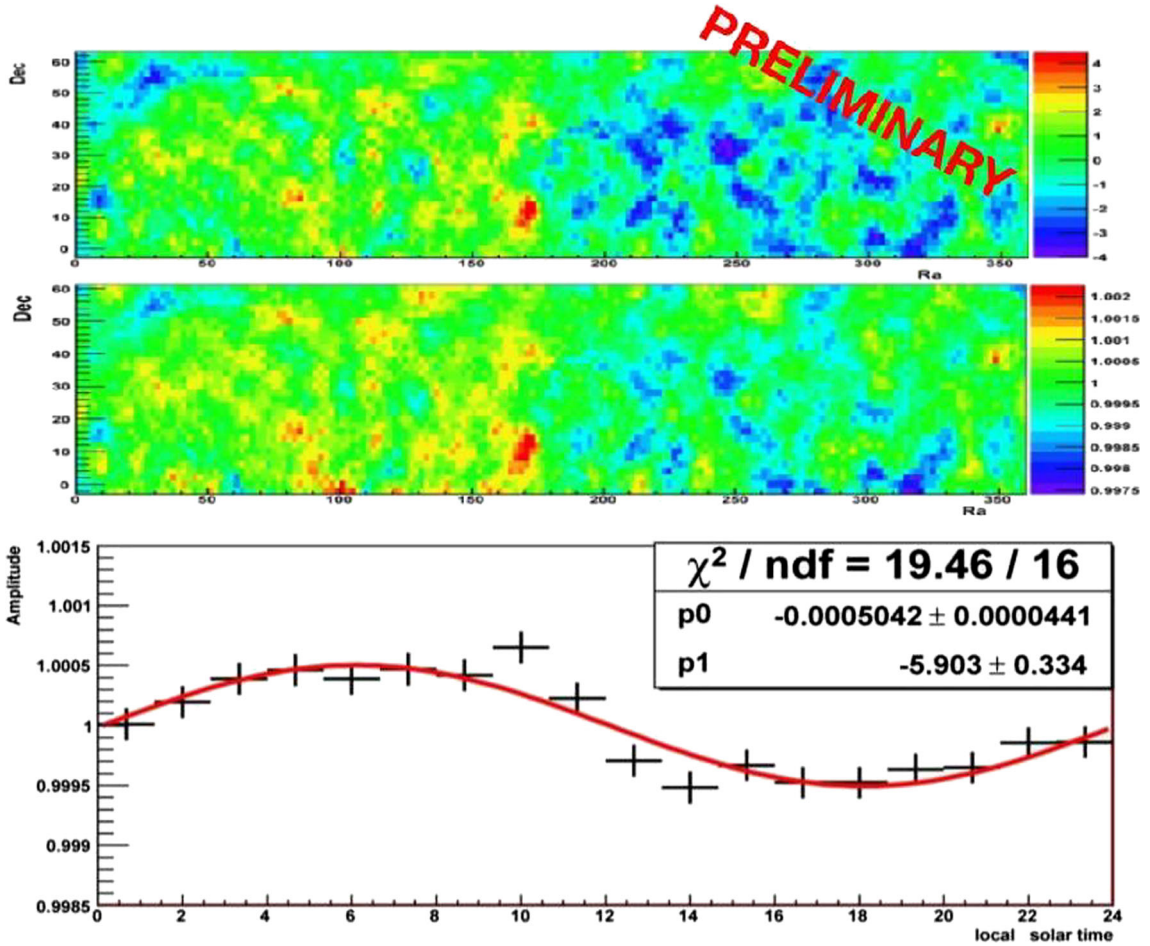

Fig. 9 Compton-Getting effect observed using the high-energy events, i.e., $N_{hit} > 500$, taken in 2008 and 2009 when the solar activity was low. The *upper panel* is the significance map of the anisotropy. The *middle panel* is the map of the relative intensity of the cosmic ray flux. The *lower panel* is the phase distribution of the integral of the relative flux over the whole declination range. The *horizontal axes* of the three panels are the time in a mean solar period of 24 h

ARGO-YBJ and IceCube [31] as shown in Fig. 10a, it helps to identify the spatial locations in the sky for the two regions with clear excess and deficit. In equatorial coordinates, on the left hand side, it is clearly shown that the structure does not support a fit with a simple dipole component. In galactic coordinates, on the right-hand side, the excess is concentrated towards a direction around $-15°$ in latitude and certainly not towards the galactic center, rather close the opposite direction, or anti-galactic-center direction. Also in the galactic coordinates, the deficit, so-called "loss cone," is concentrated towards a direction of 35° in latitude, not up-right.

At smaller scales, ARGO-YBJ not only confirmed the excesses reported by MILAGRO experiment [28], referred to regions "A" and "B" there and "1" and "2" here in Fig. 10b, using the same method in the analysis for the medium-scales anisotropic structure, but also finds some excesses in new regions ("3" and "4") with significance of 7σ and 5.5σ, respectively. The corresponding intensity of the new excesses are 0.023 and 0.016 % [32]. The coincidence of the two observations with strong significance in the small regions, A and B, is remarkable. Remarkably, different techniques are used in the two experiments 7 years apart from each other. On the other hand, it is very difficult to understand what causes the excesses located at such high galactic latitudes because the rigidity of a few TV implies a very close-by origin of the excesses. There is no explanation in the literature so far.

4 Conclusions

ARGO-YBJ is a multipurpose cosmic ray and gamma ray observatory at 4,300 m a.s.l. in Tibet, China. Starting from the end of 2007, the full coverage RPC detector array of 5,600 m^2 has been very stably operated for 1,670 days. As a wide FOV and high-duty cycle astrophysical facility, ARGO-YBJ accumulated an exposure that enables the

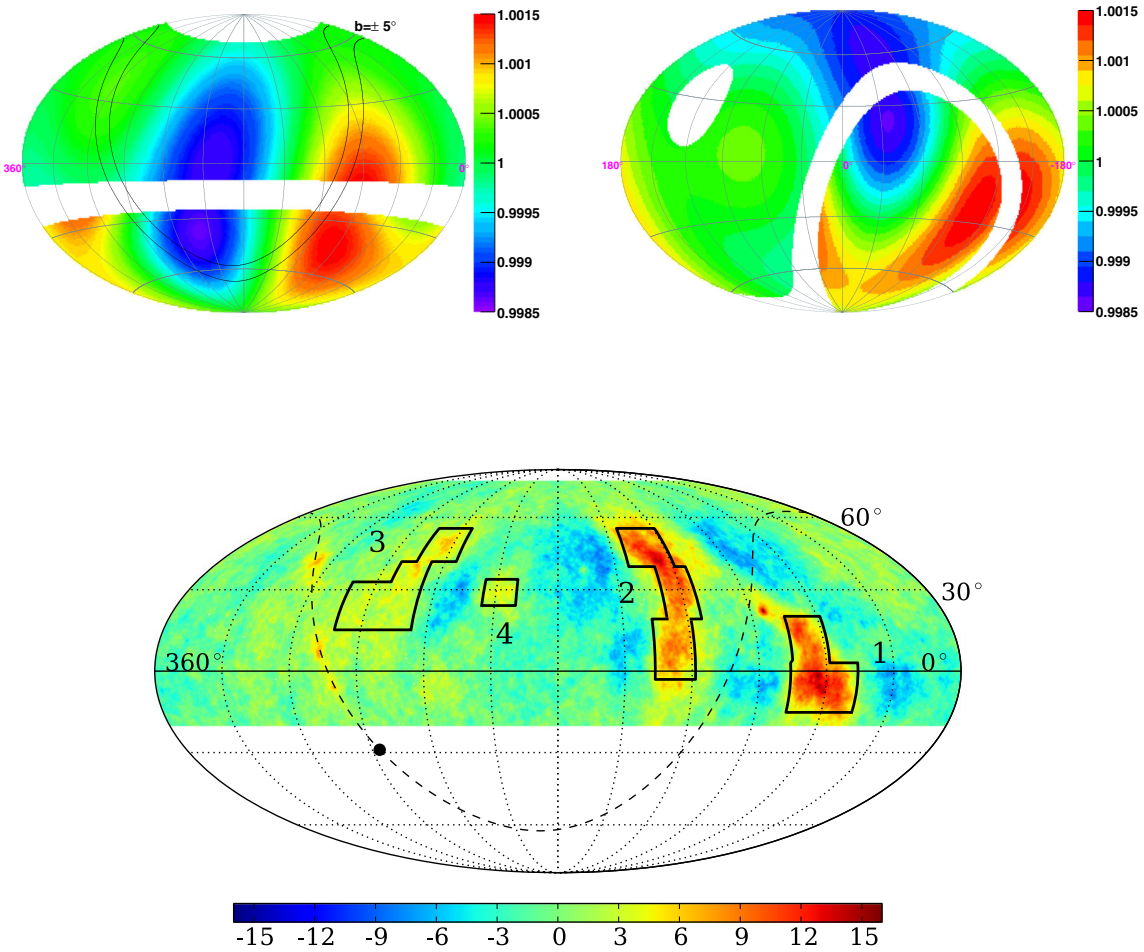

Fig. 10 The sky maps of the significance of the CR anisotropy. The *two figures* in the *upper panel* are the global map of the anisotropy of CRs at large scales using ARGO-YBJ measurement around a few TeV and IceCube measurements around 30 TeV in equatorial coordinates (*left*) and in galactic coordinates (*right*), respectively. In order to make the anisotropy at large scales more pronouncing, only dipole and quadruple components from both harmonic analysis are plotted here. The *figure* in the *lower panel* is the anisotropy sky map at medium scales over the FOV of ARGO-YBJ

observation of the standard candle Crab Nebula by a significance of 21σ. The survey depth reaches $0.24 I_{Crab}$. Among the well-observed six gamma ray sources, most galactic sources are spatially extended over sizes compatible with the ones measured by Cherenkov telescopes. ARGO-YBJ clearly measures the photon flux more completely than the narrow FOV devices, so that it is relatively more sensitive to those extended sources. Also among the observed sources, two blazars have been monitored for every flare over years. Long-term measurement of the light curves of the blazars in nearly full duty cycle enables fruitful analysis on the emitting mechanisms of gamma rays over a wide energy range using multiwavelength data. By measuring almost every charged particle in showers, particularly near the cores, ARGO-YBJ reaches the lowest threshold energy in air shower detection so that it is able to measure the cosmic ray spectrum at energies that have been significantly covered by CREAM with a direct measurement of the spectra for all individual species. From a few TeVs up to 800 TeV, ARGO-YBJ successfully selects protons and helium nuclei out by fully taking advantage of the trigger bias towards the light components at low energies and of a multiparameter composition analysis at the high-energy part. The agreement between the ARGO-YBJ and CREAM measurements serves as a calibration of the energy scale with an accuracy of 4.5 %. With the energy resolution of 25 %, no bending, hardening, or other structure on the spectrum of protons and helium nuclei is observed up to 1 PeV. Anisotropy in cosmic ray arrival directions has been measured in many details using ARGO-YBJ due to its huge exposure. Compton-Getting effect as a well-defined modulation of the total flux at an amplitude of 0.05 % is measured as a good calibration of the detector for this dedicate purpose. A global view of the anisotropy at large scale has been reported by combining the ARGO-YBJ and IceCube measurements together. In the 2D sky map, the

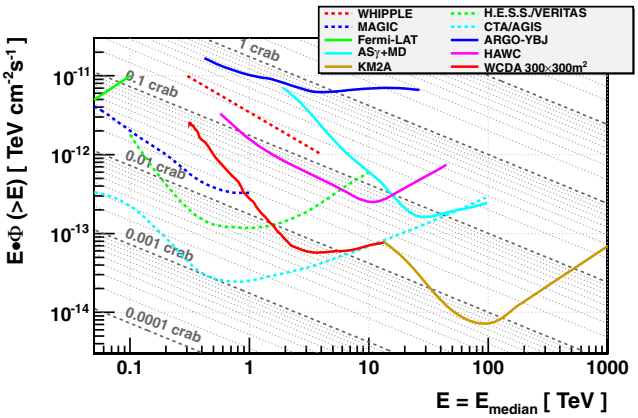

Fig. 11 The sensitivity of LHAASO in *red and golden*. *Solid curves* for other surveying experiments and projects and *dashed curves* for Cherenkov telescope experiments and projects are plotted here in the same figure for comparison. The exposure for wide field-of-view detectors and IACTs is 1 year and 50 h, respectively

directions of the deficit and excess regions are defined. The anisotropy structures at smaller scales are also measured by using ARGO-YBJ data. Not only confirms the "medium-size hot spots" observed by MILAGRO, ARGO-YBJ also finds some new features of the map of the anisotropy.

Together with the MILAGRO experiment, ARGO-YBJ demonstrates the power of the EAS detector arrays as a wide FOV surveying technique for gamma ray sources. The only key piece still missing is the sufficient sensitivity of these devices. Currently, HAWC is under construction and is going to boost the surveying sensitivity to a level of 0.1 Crab unit by the end of year 2014. Further on the horizon, LHAASO will be built with an improvement in survey sensitivity by a factor of 3 or larger. Moreover, LHAASO will have a capability to measure energy spectra of close sources up to 1 PeV, thus may identify some barionic pevatrons in our galaxy. The estimated sensitivity of LHAASO is shown in Fig. 11 as a function of the gamma ray energy. All major projects are included in the figure for comparison. It is obvious that LHAASO will be useful for improving all cosmic ray related measurements mentioned in this paper.

Acknowledgments This work is supported in China by NSFC (Nos. 10120130794, 11205165, 10975145, and 11075170), the Chinese Ministry of Science and Technology, the Chinese Academy of Sciences, the Key Laboratory of Particle Astrophysics, CAS, and in Italy by the Istituto Nazionale di Fisica Nucleare (INFN). We also acknowledge the essential supports of W.Y. Chen, G. Yang, X.F. Yuan, C.Y. Zhao, R. Assiro, B. Biondo, S. Bricola, F. Budano, A. Corvaglia, B. DAquino, R. Esposito, A. Innocente, A. Mangano, E. Pastori, C. Pinto, E. Reali, F. Taurino and A. Zerbini, in the installation, debugging, and maintenance of the detector.

References

1. G. Aielli et al., Nucl. Instrum. Meth. A. **562**, 92 (2006)
2. G. Aielli et al., Nucl. Instrum. Meth. A. **608**, 246 (2009)
3. P. Creti et al., 29th ICRC, Pune, 97 (2005)
4. G. Aielli, et al., Nucl. Instrum. Meth. Phys. Res. A. in press
5. B. Bartoli et al., Astrophys. J. **734**, 110 (2011)
6. B. Bartoli et al., Phys. Rev. **D84**, 022003 (2011)
7. G. Aielli et al., Nucl. Instrum. Meth. A. **661**, S50 (2012)
8. B. Bartoli et al., Astrophys. J. **760**, 110 (2012)
9. M. Ackermann1 et al. Sci. **334**, 1103 (2011)
10. B. Bartoli et al., Astrophys. J. **767**, 99 (2013)
11. M. Ackermann et al., Astropart. Phys. **518A**, 71 (2012)
12. A. A. Abdo et al., Astrophys. J. **688**, 1078 (2008)
13. S. LeBohec, I. H. Bond, S. M. Bradbury et al., Astrophys. J. **539**, 209 (2000)
14. F. Aharonian et al., A&A. **375**, 1008 (2001)
15. B. Bartoli et al., Astrophys. J. **734**, 110 (2011)
16. B. Bartoli et al., Astrophys. J. **758**, 2 (2012)
17. B. Bartoli et al., Astrophys. J. in press
18. H. S. Ahn et al., Astrophys. J. **714**, L89 (2010)
19. J. R. Horandel, Astropart. Phys. **19**, 193 (2003)
20. B. Bartoli et al., Phys. Rev. **D85**, 092005 (2012)
21. S. S. Zhang et al., Nucl. Instr. and Meth. A. **629**, 57 (2011)
22. S. S. Zhang et al., Energy spectrum of cosmic Protons and Helium nuclei with a hybrid measurement by ARGO-YBJ and a wide field Cherenkov telescope, 33rd ICRCRIO DE JANEIRO (2013)
23. T. Antoni et al., Astropart. Phys. **24**, 1 (2005)
24. M. Amenomori et al., Adv. Space Res. **47**, 629 (2011)
25. M. Amenomori et al., Phys. Rev. **D62**, 112002 (2000)
26. A. DAmone et al., "Mass composition and hadronic interaction studies with ARGO-YBJ", 33rd ICRCRIO DE JANEIRO (2013)
27. M. Amenomori et al., Sci. **314**, 439 (2006)
28. A. A. Abdo et al., Astrophys. J. **698**, 2121 (2009)
29. R. Abbasi et al. Astrophys. J. **718**, L194 (2010)
30. A. H. Compton, I. A. Getting, Phys. Rev. Lett. **47**, 817 (1935)
31. S. Toscano, (for the IceCube Collaboration). arXiv:1011.5428v1 [astro-ph.HE]
32. B. Bartoli et al., Prys. Rev. **D88**, 082001 (2013)
33. F. A. Aharonian, A. Akhperjanian, M. Beilicke, et al., ApJ. **614**, 897 (2004)
34. J. Albert, E. Aliu, H. Anderhub, et al., ApJ. **674**, 1037 (2008)
35. M. Amenomori, X. J. Bi, D. Chen, et al., ApJ. **692**, 61 (2009)